Insertion of the Biogenesis Factor Rei1 Probes the Ribosomal Tunnel during 60S Maturation

Basil Johannes Greber[1,6,*], Stefan Gerhardy[2,*], Alexander Leitner[3], Marc Leibundgut[1], Michèle Salem[4], Daniel Boehringer[1], Nicolas Leulliot[4], Ruedi Aebersold[3,5], Vikram Govind Panse[2,†], Nenad Ban[1,†]

[1] Institute of Molecular Biology and Biophysics, Department of Biology, ETH Zurich, CH-8093 Zurich, Switzerland

[2] Institute of Biochemistry, Department of Biology, ETH Zurich, CH-8093 Zurich, Switzerland

[3] Institute of Molecular Systems Biology, Department of Biology, ETH Zurich, CH-8093 Zurich, Switzerland

[4] Laboratoire de Cristallographie et RMN Biologiques, UMR CNRS 8015, Université Paris Descartes, Sorbonne Paris Cité, Faculté de Pharmacie, 75006 Paris, France

[5] Faculty of Science, University of Zurich, Zurich, Switzerland

[6] Current address: California Institute of Quantitative Biosciences (QB3), University of California Berkeley, Berkeley, CA 94720-3220, U. S. A.

[†] Correspondence should be addressed to N.B. (ban@mol.biol.ethz.ch) or V.G.P. (vikram.panse@bc.biol.ethz.ch).

[*] These authors contributed equally to this work.

SUMMARY

Eukaryotic ribosome biogenesis depends on several hundred assembly factors to produce functional 40S and 60S ribosomal subunits. The final phase of 60S subunit biogenesis is cytoplasmic maturation, which includes the proofreading of functional centers of the 60S subunit and the release of several ribosome biogenesis factors. Here we report the cryo-EM structure of the yeast 60S subunit in complex with the biogenesis factors Rei1, Arx1, and Alb1 at 3.4 Å resolution. In addition to the network of interactions formed by Alb1, the structure reveals a mechanism for ensuring the integrity of the ribosomal polypeptide exit tunnel. Arx1 probes the entire set of inner ring proteins surrounding the tunnel exit, and the C-terminus of Rei1 is deeply inserted into the ribosomal tunnel where it forms specific contacts along almost its entire length. We provide genetic and biochemical evidence that failure to insert the C-terminus of Rei1 precludes subsequent steps of 60S maturation.

INTRODUCTION

Mature and functionally active 40S and 60S ribosomal subunits that assemble with messenger RNA and transfer RNAs (tRNA) to form translating 80S ribosomes are responsible for cellular protein synthesis in eukaryotes (Klinge et al., 2012). These complex ribonucleoprotein assemblies are produced in a highly intricate and tightly controlled pathway termed ribosome biogenesis (Gerhardy et al., 2014). Ribosome biogenesis starts in the nucleolus, where ribosomal RNAs (rRNAs) are transcribed and assembled with early-binding ribosomal proteins. Biogenesis of the 60S ribosomal subunit proceeds through several assembly, remodeling and rRNA processing steps in the nucleolus and the nucleoplasm before the nascent pre-60S particle can be exported into the cytoplasm (Gerhardy et al., 2014). Nuclear export is a key step in ribosome biogenesis and requires the recruitment of several nuclear export factors that mediate interactions with FG-repeat nucleoporins, including Arx1 (Bradatsch et al., 2007; Hung et al., 2008), Nmd3-Crm1 (Ho et al., 2000), Mex67-Mtr2 (Yao et al., 2007), Bud20 (Altvater et al., 2012; Bassler et al., 2012), and Ecm1 (Yao et al., 2010) in

yeast. After nuclear export, pre-60S particles need to be functionally activated for their role in translation (Panse and Johnson, 2010). This process is termed cytoplasmic maturation and proceeds through an ordered series of events, which include the release of many ribosome biogenesis factors and the incorporation of the last remaining ribosomal proteins (Gerhardy et al., 2014; Lo et al., 2010). Several proofreading steps ensure that the functional centers of the 60S subunit, such as the ribosomal stalk (Kemmler et al., 2009; Lo et al., 2010; Lo et al., 2009) and the peptidyl transferase (PTC) active site (Bussiere et al., 2012), are properly assembled. However, there are currently no structural insights into these processes, and no mechanism that would ensure proper assembly of the ribosomal polypeptide exit tunnel, which is a critical architectural feature of the ribosome, has been proposed yet.

The cytoplasmic zinc finger protein Rei1 (Hung and Johnson, 2006; Iwase and Toh-e, 2004; Lebreton et al., 2006; Meyer et al., 2010), the J-domain protein Jjj1 (Demoinet et al., 2007; Meyer et al., 2010; Meyer et al., 2007) and the Hsp70-type ATPase Ssa (Lo et al., 2010; Meyer et al., 2007) are required to release the nuclear export factor Arx1 during cytoplasmic maturation of the 60S subunit. Arx1 is structurally homologous to methionine amino peptidase (MAP) enzymes (Giglione et al., 2004; Hung and Johnson, 2006; Kowalinski et al., 2007) and binds the pre-60S subunit near the polypeptide tunnel exit site (Bradatsch et al., 2012; Greber et al., 2012; Hung and Johnson, 2006). While Rei1 is required for Arx1 release *in vivo*, it has also been shown to increase the affinity of Arx1 for the 60S particle *in vitro* (Greber et al., 2012). How Rei1 mediates both of these disparate and seemingly opposing functions remains to be established. Mutations in Rei1 and Jjj1 lead to accumulation of Arx1 on pre-60S subunits in the cytosol (Hung and Johnson, 2006; Lo et al., 2010; Meyer et al., 2010; Meyer et al., 2007) and block downstream pre-60S maturation events, including the release of the anti-association factor Tif6p (the yeast homolog of human eIF6) from the interface side of the 60S subunit (Lebreton et al., 2006; Lo et al., 2010). These defects can be alleviated by deletion of Arx1 (Hung and Johnson, 2006; Lebreton et al., 2006; Lo et al., 2010) or Alb1 (Demoinet et al., 2007; Lebreton et al., 2006; Meyer et al., 2007), a small, highly positively charged protein that

forms a stable complex with Arx1 and is thereby recruited to the maturing pre-60S particle in the nucleoplasm (Bradatsch et al., 2007; Bradatsch et al., 2012; Lebreton et al., 2006). These observations indicate that events at the tunnel exit are coordinated with maturation steps at the subunit interface, and that the presence of Arx1 and Alb1 is inhibitory to downstream maturation. It was initially proposed that the Arx1-Alb1 heterodimer accumulates as a soluble complex in the cytosol in Rei1 or Jjj1 mutant cells (Demoinet et al., 2007; Lebreton et al., 2006), however more recent data indicate that the Arx1-Alb1 complex remains bound to the pre-60S particle under these conditions, suggesting that the persistence of the Arx1-Alb1 dimer on the pre-60S particle is the cause for the inhibition of downstream maturation (Lo et al., 2010; Meyer et al., 2010). The mechanism by which this coordination between Arx1-Alb1 release and later steps of pre-60S biogenesis is achieved has remained elusive.

Cryo-electron microscopy (cryo-EM) studies of a native yeast pre-ribosomal particle purified by tandem affinity purification (TAP) (Bradatsch et al., 2012; Leidig et al., 2014) as well as *in vitro* reconstituted complexes of the mature 60S subunit with Arx1, Rei1, and Jjj1 (Greber et al., 2012) showed that Arx1 is bound near the polypeptide tunnel exit site of the 60S subunit. Arx1 has been suggested to support the nuclear export of the pre-60S particle in yeast by interacting with FG-repeat nucleoporins in a cavity corresponding to the catalytic pocket in the homologous MAP enzymes (Bradatsch et al., 2007). However, the cryo-EM structures showed that access to this cavity is restricted in 60S-bound Arx1 because it faces the ribosomal surface (Bradatsch et al., 2012; Greber et al., 2012). The solvent-exposed side of Arx1 interacts with expansion segment (ES) 27 and thereby stabilizes this long eukaryotic-specific rRNA helix (Greber et al., 2012). Intriguingly, the *in vitro* reconstituted 60S-Arx1-Rei1 complex showed a rod-like density at the end of the polypeptide exit tunnel, suggesting that one of the bound biogenesis factors might be involved in the proofreading of the conformation of the exit region of the ribosomal tunnel (Greber et al., 2012).

Here we report the cryo-EM structure of the 60S-Arx1-Alb1-Rei1 complex at near-atomic resolution, which allowed us to build an almost complete atomic

model of Arx1, map its interactions with the 60S subunit, and identify the localization of Alb1. Furthermore, we were able to perform a detailed functional and structural interpretation of the structure of the C-terminus of Rei1, which is inserted into the ribosomal polypeptide exit tunnel and extends almost along its entire length to reach within 15 Å of the PTC active site at the other end of the tunnel.

RESULTS

The structure of the 60S-Arx1-Alb1-Rei1 complex

To enable a detailed structural analysis of the network of interactions of ribosome biogenesis factors near the ribosomal tunnel exit, we *in vitro* reconstituted the complex of the yeast 60S subunit with Rei1 and the Arx1-Alb1 heterodimer. The mature 60S particle can serve as a model substrate because Rei1 binding and Arx1-Alb1 release occur on late cytoplasmic 60S biogenesis intermediates, which are nearly fully assembled and contain fully processed rRNAs (Gerhardy et al., 2014). The *in vivo* release reactions during final cytoplasmic 60S maturation are therefore likely reversible and equivalent to the *in vitro* binding reactions, an idea that is consistent with the observation of binding of biogenesis factors to mature 60S subunits *in vivo* (Merl et al., 2010). To improve solubility of the protein, Alb1 carried an N-terminal maltose-binding protein (MBP) fusion, and Rei1 carried a C-terminal hexahistidine (H_6) tag. We determined the structure of the 60S-Arx1-Alb1-Rei1H_6 complex at near-atomic resolution using cryo-EM (**Figure 1, Figure S1**), revealing the structure of the 60S subunit with the biogenesis factors bound near the exit of the polypeptide tunnel, in agreement with previous results at lower resolution (Bradatsch et al., 2012; Greber et al., 2012). A reconstruction representing a major particle population with ES27 occupying the so-called tunnel conformation and contacting Arx1 was resolved to 3.4 Å resolution (**Figure S2A**), while a second population with bound Arx1 and poorly ordered ES27 partially occupying the alternative L1 conformation was resolved to 3.7 Å resolution (**Figure S1B**). The latter state has not been observed in 60S-Arx1-Rei1H_6 complexes lacking Alb1

(Greber et al., 2012). Further analysis will focus on the more highly resolved state with ES27 in the tunnel conformation.

The near-atomic resolution cryo-EM map of the 60S-Arx1-Alb1-Rei1H_6 complex with ES27 in the tunnel conformation shows density for all three bound biogenesis factors (**Figure 1**). The N-terminal MBP-tag on Alb1 was not visualized in the map, likely due to flexibility. Much of the ribosomal core is resolved at close to 3.0 Å resolution while Arx1 and parts of Rei1 are resolved to 3.5-4.0 Å (**Figure S2C-E**), which permits atomic model building, refinement, and validation (**Figure S2**, **Tables S1**, **S2**). Peripheral parts of Alb1 and ES27 are less well ordered and could not be interpreted by a full atomic model (**Figure S2C**).

The structure of Rei1

Rei1 is a 393 amino acid (aa) protein containing three zinc finger domains (Iwase and Toh-e, 2004). Our 3.4 Å-resolution structure reveals that the region of Rei1 that was visualized previously at lower resolution (Greber et al., 2012) corresponds to the middle part (residues 145-261) of the Rei1 sequence and encompasses the second and third zinc fingers of the protein, which are wedged in between rRNA ES41 and ribosomal protein eL22 (**Figure 1, Figure 2A**). ES41 is bent towards the subunit interface side in a conformation that is probably incompatible with the formation of the translating 80S ribosome due to clashes with protein eS8 of the 40S subunit (**Figure 2B**). This interaction may therefore enable Rei1 to preferentially bind to 60S subunits (Hung and Johnson, 2006; Parnell and Bass, 2009). Residues 1-144 of the protein, which include the first zinc finger, are not visualized in the map and may therefore be disordered. The location of the N-terminus of the visible part of Rei1 suggests that this N-terminal domain may be located close to ES41 and ribosomal protein eL24. While residues 262-298 are also not well ordered, the C-terminal 95 aa of Rei1 (residues 299-393) could again be interpreted at atomic level. This part of the protein stretches across rRNA helix (H) 59 to Arx1 (**Figure 2C**) and then further into the polypeptide tunnel exit (**Figure 2D, E**), where excellent side chain features become visible due to higher local resolution (**Figure S2E**). These side-

chain features establish unambiguously that the C-terminus of Rei1 is inserted into the polypeptide tunnel (**Figure 2F, G**) and reaches from the tunnel exit site towards the PTC (**Figure 2H**).

During cytoplasmic maturation of the pre-60S particle, the loading of Rei1 appears to be coupled to the loading of eL24 after Drg1-dependent removal of the eL24 placeholder Rlp24 (Lo et al., 2010; Pertschy et al., 2007). While previous data indicated that Rei1 residues near the C-terminus might interact with eL24 (Demoinet et al., 2007; Lebreton et al., 2006), our structural data suggest that the Rei1 N-terminal domain may approach eL24. However, possible interactions in this area have not been visualized in our cryo-EM map and may depend on the presence of other biogenesis factors in the native pre-60S particle, which are absent in the *in vitro* reconstituted complex.

While our highest-quality structure is derived from a complex assembled using C-terminally H_6-tagged Rei1 (Rei1H_6), the H_6-tag of which is partially visualized in the cryo-EM density, we also confirmed our mapping of the Rei1 C-terminus using an N-terminally H_6-tagged Rei1 construct (H_6Rei1), resulting in a native C-terminus (**Figure S3**, **Table S2**). The density for Rei1, including the section inserted into the tunnel, is highly similar between the two complexes, except for the segment corresponding to the H_6-tag of Rei1H_6, which is missing in the H_6Rei1 reconstruction (**Figure S3D, E**), and the last three residues of Rei1, which occupy a different conformation in the absence of the H_6-tag (**Figure S3F**).

Interactions of Rei1 inside the polypeptide exit tunnel

A total of 35 aa of Rei1 are inserted into the polypeptide exit tunnel, reaching across the constriction site formed by loops of ribosomal proteins uL22 and uL4 and to within 15 Å of the peptidyl transferase (PTC) active site at the other end of the tunnel (**Figure 2D, H**). The very C-terminal segment of Rei1, closest to the PTC, adopts an elongated conformation and follows the path of the tunnel. This part of Rei1 forms close contacts with both the rRNA of the tunnel wall and ribosomal proteins uL4 and uL22 near the constriction site (**Figure 2F**, **G**, **Figure**

S4A-F). A Q-X-H-F/Y-R-X-Q motif conserved between yeast and humans (**Figure S4G**) is located at the entrance of the constriction site on the side facing the PTC (**Figure 2F, G**) and mediates a number of these interactions (**Figure S4A, B**). The conserved residues H386 and R388 interact with the backbone of the 25S rRNA by ionic and stacking interactions, respectively (**Figure S4A, B**), while Q384 and Y387 are positioned in proximity of the interface between uL22 and the 25S rRNA. Closer to the polypeptide tunnel exit site, Rei1 forms an α-helix of approximately 25 aa (**Figure 2E**), which interacts with the tunnel wall via a stacking interaction between W363 and the base of 25S rRNA A1503 (**Figure S4C, F**), as well as via several positively charged residues, of which only K371 and R367 facing protein uL22 are conserved (**Figure S4G**). Just outside of the tunnel, a short linker connects the α-helix in the tunnel to the penultimate α-helix of Rei1 (residues 334-342), which is sandwiched between the main fold and the most N-terminal helix of Arx1 (**Figure 2C**). This interaction may tether Arx1 to the 60S subunit, rationalizing the increased salt stability and affinity of Arx1 binding to the 60S subunit in presence of Rei1 (Greber et al., 2012).

Functional Analysis of the Rei1 sensor domain

In order to test whether the insertion of the C-terminal domain of Rei1 into the polypeptide tunnel is important for 60S biogenesis, we constructed mutant yeast strains harboring Rei1 variants with a bulky moiety in the form of a TAP-tag (Rigaut et al., 1999) or green fluorescent protein (GFP) fused to the Rei1 C-terminus. Both of these moieties contain a folded domain, which cannot be inserted into the polypeptide exit tunnel, leading to the exposure of the C-terminal domain of 60S-bound Rei1. Consistent with an important function of the insertion of the Rei1 C-terminal domain into the ribosomal tunnel, these yeast mutants showed a pronounced growth defect at low temperatures (**Figure 3A**). Fluorescence microscopy and sucrose density gradient centrifugation experiments using cells expressing Rei1-TAP and Rei1-GFP show that Arx1 and Tif6 are mislocalized to the cytoplasm and that 60S subunit biogenesis is affected in these cells, leading to formation of half-mers in the sucrose gradient profiles (**Figure 3B, C**). It appears that in our mutant strains, initial cytoplasmic release

events, such as Nog1 release and the stalk assembly branch of cytoplasmic maturation (Lo et al., 2010), including release of Mrt4 (Kemmler et al., 2009; Lo et al., 2009) (**Figure 3C, D**), proceed normally, while maturation events near the tunnel exit are impaired, thus blocking downstream maturation (**Figure 3D**). This indicates that the C-terminus of Rei1 may function as a sensor domain, and that its insertion into the ribosomal tunnel may serve a proofreading role to test the integrity of the tunnel.

To investigate the precise role of the sequence elements inside the tunnel, we constructed Rei1 variants bearing deletions at the C-terminus, ranging from short four-amino-acid deletions to deletion of the entire C-terminal segment including the 25 aa α-helix that binds inside the exit region of the tunnel. Because the Rei1 homolog Reh1, which bears a C-terminal region with high homology to the C-terminus of the Rei1 sensor domain (**Figure 4A**), might play a partially redundant role (Parnell and Bass, 2009), we constructed a *rei1Δ* P_{GAL1}-Reh1 yeast strain, where in addition to the genomic deletion of Rei1, Reh1 can be depleted by growing the cells on glucose medium. In agreement with previous reports of a synthetic growth defect between Rei1 and Reh1 (Iwase and Toh-e, 2004; Parnell and Bass, 2009), the *rei1Δ* P_{GAL1}-Reh1 strain showed a severe growth defect on glucose medium (**Figure 4B**), indicating that Rei1 and Reh1 perform an overlapping but highly important cellular function. We then introduced full-length Rei1 and the Rei1 C-terminal deletion variants into this strain. While full-length Rei1 restored growth of the cells to wild-type level, introduction of a Rei1 variant lacking 8 aa at the C-terminus, which are part of the conserved C-terminal Q-X-H-F/Y-R-X-Q motif (**Figure S4**), only partially complemented the growth defect (**Figure 4C**). Interestingly, this growth defect was not exacerbated by further deletion of the remainder of the Rei1 segment inserted into the tunnel (**Figure 4C**), indicating that in the context of the tunnel-inserted state, residues 355-385 might act as a spacer to allow the access of the highly conserved C-terminus to its binding site inside the ribosomal tunnel. Our experiments also indicate that the short Rei1 helix that interacts with Arx1 (**Figure 2C**) is functionally important, as both a truncated Rei1 variant lacking

this helix and a mutant in which it is replaced by a $(Ser\text{-}Gly)_5$-Ser linker show a strong growth defect (**Figure 4C**).

Notably, the presence of the exposed Rei1 C-terminal domain unable to become inserted into the polypeptide tunnel (**Figure 3A**) induces a more severe growth defect than the deletion of this segment (**Figure 4C**), indicating that the Rei1 C-terminal sensor domain may act as a negative regulator of Arx1 release and pre-60S maturation upon exposure. Furthermore, the C-terminal region of Rei1 may be functionally important, possibly in signaling through the polypeptide exit tunnel or to specifically test the integrity of the constriction site, which might be particularly prone to misfolding. Indeed, the existence of a checkpoint monitoring the integrity of the loop of protein uL4 forming part of the tunnel wall at the constriction site has been proposed recently (Stelter et al., 2015). Activation of this checkpoint leads to accumulation of late pre-60S biogenesis intermediates (Stelter et al., 2015), consistent with our observations indicating a 60S biogenesis defect and impaired Arx1 and Tif6 (eIF6) recycling to the nucleus in the Rei1-TAP or Rei1-GFP mutant yeast strains (**Figure 3B-D**).

The structure of Arx1 and its interactions with the 60S subunit

Structures of Arx1 proteins from thermophilic fungi (van Noort et al., 2013) and the mammalian homolog Ebp1 (Kowalinski et al., 2007) have been solved by X-ray crystallography, confirming that Arx1 harbors a conserved type-2 methionine aminopeptidase core fold (Giglione et al., 2004; Kowalinski et al., 2007). However, yeast Arx1 contains several sequence insertions that are not found in these homologous proteins, and correspondingly, considerable portions of the Arx1 density in previous lower-resolution cryo-EM reconstructions, among them several interaction sites with the 60S subunit, remained unassigned (Bradatsch et al., 2012; Greber et al., 2012). We were able to build and refine a near-complete structure of yeast Arx1 based on our cryo-EM map of the 60S-Arx1-Alb1-Rei1H_6 complex (**Figure 5A**), revealing the structure and organization of the yeast Arx1 extensions in comparison to the type-2 MAP core fold (**Figure 5B**). Most of these extensions have no structural equivalents in the

Arx1 protein of the thermophilic fungus *Chaetomium thermophilum* (**Figure 5C**). Several of them fold into additional secondary structure elements that extend the core fold of Arx1 and are involved in the interaction of Arx1 with the functionally important region of the 60S subunit near the polypeptide tunnel exit and with ES27 (**Figure 5D-F**). Consistent with the previous analysis of lower-resolution cryo-EM maps (Bradatsch et al., 2012; Greber et al., 2012), the access to the space between the ribosomal surface and the Arx1 core fold, and therefore to the polypeptide tunnel exit and the putative nucleoporin binding pocket of Arx1 (Bradatsch et al., 2007), is strongly restricted, with Arx1 extensions contributing most of the lateral shielding (**Figure 5E, F**). Only one significant access window remains (**Figure 5E**), which is required for Rei1 to insert its C-terminal sensor domain into the ribosomal tunnel.

The type 2 MAP-like core domain of Arx1 interacts with 25S rRNA H59 and ES27 as well as ribosomal proteins uL23 and eL19. Arx1 extensions additionally interact with uL24, uL29, and H7 of the 5.8S rRNA, and also contribute to the interaction with ES27 (**Figure 5G, H**). Two major areas of electropositive potential on Arx1 are involved in ribosomal interactions (**Figure S4H**). One of them is composed of Arx1 residues in the region of residues 79-84 and 570-580 and localizes to the upper surface of Arx1 where it interacts with ES27 (**Figure S4H**), while the other involves a subdomain specific to type 2 MAPs but absent in type 1 MAPs, which forms the interaction in the region of H59, uL23, and eL19 (**Figure 5H**). In addition to mediating electrostatic interactions, this region of Arx1 also provides a binding pocket for U1763 of the 25S rRNA, which forms part of the hairpin loop at the tip of H59 (**Figures 5I, S4I**). The overall structure as well as the positive electrostatic potential in this region are conserved between Arx1 and type 2 MAP (**Figure S4J**), which is also ribosome-binding (Raue et al., 2007). These observations provide additional support for the idea that Arx1 and type 2 MAP use this domain to mediate ribosome interactions by formation of a number of conserved contacts, positioning them similarly above the ribosomal tunnel (Greber et al., 2012).

Identification of Alb1 and its interactions with Arx1 and the 60S subunit

To reliably identify density belonging to Alb1 in the 60S-Arx1-Alb1-Rei1H_6 complex, we determined the cryo-EM structure of a 60S-Arx1-Rei1H_6 complex in the absence of Alb1 at 3.7 Å resolution (**Figure S5**). The comparison of the cryo-EM density of this complex to the structure of the 60S-Arx1-Alb1-Rei1H_6 complex revealed three major density elements that are present in the Alb1-containing complex, but absent in the 60S-Arx1-Rei1H_6 complex (**Figure 6A**, **Figure S6**), indicating that they belong to the bound Alb1 molecule. Interestingly, these density elements are also present in the lower-resolution cryo-EM reconstructions of a pre-ribosomal particle purified by Alb1-TAP, but could not be distinguished from Arx1 in these studies due to their small size (**Figure S6**) (Bradatsch et al., 2012; Leidig et al., 2014). The arrangement of the observed segments, one β-strand and two α-helices, suggests that Alb1 does not form a compact fold, but instead is stretched out across the surface of Arx1 and the 60S subunit, with extended flexible linkers connecting the secondary structure elements (**Figure 6B**).

To confirm our assignment of these density elements to Alb1, we subjected the 60S-Arx1-Alb1-H_6Rei1 complex and two variants of the isolated Arx1-Alb1 complex, once with and once without an MBP-tag fused to the Alb1 N-terminus, to chemical crosslinking/mass spectrometry (CX-MS) (Walzthoeni et al., 2013). The isolated Arx1-Alb1 complexes showed crosslinking of one region of Alb1 to several widely distributed sites of Arx1, indicating high conformational flexibility of this region of Alb1 in solution. CX-MS analysis of the 60S-containing sample, in contrast, yielded crosslinks between ribosomal proteins that are consistent with prior structural knowledge of the 60S subunit (Ben-Shem et al., 2011), as well as crosslinks of Arx1 and Alb1 to the 60S subunit that are in good overall agreement with our structural data of the 60S-Arx1 interaction and the density features attributed to Alb1 (**Figure 6B, Figure S6, Table S3**). While the CX-MS data confirm our assignment of density elements to Alb1, the quality of the Alb1 density is insufficient to assign the sequence register or unambiguously establish the location of the N- or C-termini of the protein. Therefore, we modeled only the

protein backbone and restrict our interpretations to secondary structure elements.

Two elements of the Alb1 density correspond to structural elements interacting with Arx1 by formation of an interprotein β-sheet with Arx1 residues 536-539, and via an α-helix that fits into a groove formed by Arx1 extensions (**Figure 6C**). The remaining observed density element of Alb1 corresponds to two α-helices that interact with the 60S subunit rRNA. Even though not well ordered in our cryo-EM map, it appears that some segments in this region of Alb1 interact with ES7A, a mostly helical segment of rRNA that is part of ES7, a large expansion segment that encompasses roughly 200 nucleotides in yeast (**Figure 6D**). The Arx1-Alb1 complex thereby bridges ES27 and ES7, two of the largest expansion segments of the yeast 60S subunit. However, given the size and fold of ES7, and the amount of protein and rRNA interactions involving this ES, Alb1 does not influence the conformation of ES7 in a way comparable to the large-scale conformational stabilization of ES27 by Arx1. Instead, the primary function of Alb1 may be to modulate the interaction of Arx1 with the 60S subunit, a hypothesis that agrees with the observation that Alb1 deletion can rescue the Arx1 recycling defect in Rei1 and Jjj1 mutant yeast cells (Lebreton et al., 2006; Meyer et al., 2007).

DISCUSSION

Proofreading of the nascent polypeptide exit tunnel and late cytoplasmic maturation of the pre-60S subunit

Our structures show that Rei1 deeply inserts its C-terminal sensor domain into the polypeptide exit tunnel and, in a manner unprecedented for ribosome associated factors, extends from the tunnel exit towards the PTC active site and reaches across the constriction site of the ribosomal tunnel. The Rei1 C-terminal sensor domain binds stably inside the tunnel and is therefore unlikely to form the same interactions with the tunnel walls as a rapidly moving nascent polypeptide would. However, Rei1 and nascent polypeptides share the same

directionality of the polypeptide, with the N-terminus facing the tunnel exit and the C-terminus oriented towards the PTC, and can sample a similar conformational space. The Rei1 C-terminus is therefore probably able to check whether the nascent polypeptide tunnel is properly assembled and folded to permit the passage of a protein chain, thereby ensuring that 60S subunits entering the pool of translating ribosomes contain no structural perturbations that would prevent a nascent polypeptide from passing through the tunnel. Our data also provides direct experimental evidence that α-helical secondary structure elements can fold within the ribosomal tunnel and that the eukaryotic ribosomal tunnel can accommodate an α-helix of at least 6 complete helical turns.

Based on our yeast genetics data that show a severe growth defect when Rei1 is fused to a bulky domain at its C-terminus (**Figure 3A**) and the mislocalization of Arx1 and Tif6 (eIF6) observed in our fluorescence microscopy experiments (**Figure 3C**), we suggest that cytoplasmic maturation becomes blocked if the Rei1 C-terminus cannot be inserted into the polypeptide tunnel of a nascent 60S particle. The fact that this growth defect is more pronounced compared to the defect upon complete removal of the Rei1 C-terminal domain (**Figure 4C**) indicates that the exposed Rei1 C-terminal region serves as a negative regulator of cytoplasmic maturation of the 60S subunit. According to this model, the exposed Rei1 C-terminal domain would inhibit Arx1 release and downstream 60S maturation in response to a blocked or misfolded polypeptide exit tunnel (**Figure 7A**). The observation that recycling of Mrt4, a protein that is released upon incorporation of ribosomal protein uL10 at the ribosomal stalk base (Kemmler et al., 2009; Lo et al., 2009), remains unaffected in the Rei1-TAP mutants (**Figure 3C**) suggests that the pathway leading to Arx1 and Tif6 (eIF6) release is compromised specifically, while stalk assembly remains possible in these mutants.

It is interesting to note that after insertion of its C-terminus into the polypeptide exit tunnel, Rei1 approaches the subunit interface side of the 60S particle from two sides (**Figure 7B**) – its C-terminus is located near the PTC while its central

region has been visualized near ES41. Its N-terminus, including the first zinc finger domain, is not resolved in our cryo-EM map but may further extend towards eL24 on the subunit interface side according to the overall orientation of Rei1 in our structure. This hypothesis is in agreement with the previously observed functional coupling between Rei1 and eL24 loading after the Drg1-dependent release of Rlp24 (Demoinet et al., 2007; Lebreton et al., 2006; Lo et al., 2010; Pertschy et al., 2007). This two-pronged approach may enable Rei1 to perform a key role in the coordination of cytoplasmic maturation events at the tunnel exit and at the subunit interface side, specifically the coordination of the release of Arx1 and Tif6 (eIF6). Due to the proximity of the Rei1 C-terminus to the PTC, Rei1 might be able to form interactions to other biogenesis factors involved in late cytoplasmic maturation that bind in this area. This includes the elongation factor-like GTPase Efl1 (Ria1 in yeast), which has been suggested to probe the P-site for integrity (Bussiere et al., 2012) and the yeast homolog of human Shwachman-Bodian-Diamond Syndrome protein SBDS (Sdo1), which cooperates with Efl1 to release Tif6 (**Figure 3D**) (Finch et al., 2011; Karbstein, 2013; Menne et al., 2007).

Possible mechanisms of the removal of Arx1 and Rei1 from the pre-60S particle by Jjj1 and Ssa

During cytoplasmic maturation of the pre-60S subunit, the J-domain protein Jjj1 is required to recruit and activate the Hsp70-type ATPase Ssa, which in turn enables the release of Arx1 from the pre-60S subunit (Lo et al., 2010; Meyer et al., 2007). The details of this process are poorly understood, and the identity of the actual target protein of the Ssa-dependent remodeling step that culminates in release of Arx1 from the pre-60S subunit is unclear. Ssa might act directly on Arx1, or alternatively on Rei1 (Meyer et al., 2010). Our structural results suggest possible mechanisms (**Figure 7C**). Jjj1 binds in the immediate vicinity of the Arx1-Rei1 interaction site and close to the Rei1 linker that emanates from the polypeptide tunnel (Greber et al., 2012). Recruitment and activation of the Ssa ATPase by Jjj1 therefore likely occurs near these sites, suggesting that these structural elements of Rei1 may be involved in the Arx1 release process. The

ATPase activity of Ssa may be required to remove the Rei1 C-terminal sensor domain from the nascent polypeptide tunnel, as this plug-like structure likely has high affinity for the ribosome. According to this hypothesis, the interaction between Rei1 and Arx1 might remain intact during remodeling, and the two proteins would be removed simultaneously. Alternatively, Ssa may disrupt the interaction between Arx1 and the functionally important helix formed by Rei1 residues 334-342 (**Figures 2C, 4C**), which probably stabilizes Arx1 on the ribosome. Disruption of this interaction would thus lead to dissociation of Arx1 while Rei1 would remain bound to the pre-60S particle. However, the fact that no release factor has been identified for Rei1 suggests that simultaneous release of Arx1 and Rei1 after extraction of the Rei1 sensor domain from the exit tunnel is more likely.

Multi-step proofreading of the polypeptide tunnel region

The combination of Arx1, Rei1, and Jjj1 probably serves to thoroughly check both the conductivity of the exit tunnel and the correct assembly of the protein biogenesis factor-binding platform at the tunnel exit. Arx1 forms extensive interactions with the region around the tunnel exit, which harbors the binding sites for the signal recognition particle and the translocon, two key players in co-translational membrane protein targeting (Kramer et al., 2009). Thereby, Arx1 may be able to check the correct assembly of ribosomal proteins in this region. After nuclear export, Rei1 binds and proofreads the ability of the exit tunnel to conduct nascent polypeptides. Final release of Arx1 and Rei1 requires Jjj1, which might additionally check the availability of the binding site for the ribosome associated complex RAC, a eukaryotic chaperone supporting protein biogenesis, because RAC and Jjj1 appear to be architecturally related (Kaschner et al., 2015; Leidig et al., 2013; Meyer et al., 2007; Zhang et al., 2014). The combination of 60S biogenesis factors we describe here may therefore monitor and support all aspects of polypeptide tunnel and tunnel exit assembly and function.

EXPERIMENTAL PROCEDURES

Preparation of ribosomal subunits

60S ribosomal subunits were prepared as described (Greber et al., 2012; Klinge et al., 2011; Rabl et al., 2011).

Rei1 cloning, expression and purification

Rei1-H_6 was prepared as described (Greber et al., 2012). To obtain H_6-Rei1, the Rei1 coding sequence was amplified from *S. cerevisiae* genomic DNA and cloned into the pProEx-htb vector to yield pProEx-htb-His_6-Rei1. H_6-Rei1 was expressed and purified as described for Rei1-H_6 (Greber et al., 2012).

Arx1 cloning, expression and purification

The Arx1 coding sequence was amplified from *S. cerevisiae* genomic DNA and cloned into the pET47 vector (Merck Millipore, Billerica, MA, USA). The protein was expressed using *Escherichia coli* BL21 Codon Plus (Agilent Technologies, Santa Clara, CA, USA) and purified by Nickel affinity and gel filtration chromatography. The complete purification protocol can be found in the **Supplemental Experimental Procedures**.

Cloning, expression and purification of the MBP:Alb1-Arx1 and Alb1-Arx1 complexes

Arx1 was cloned into the pET-15b (Novagen) vector with a N-terminal His-tag and Alb1 into petM41 with a His-MBP fusion at the N-terminus. The proteins were co-expressed in *E. coli* Rosetta 2 (DE3) cells. The MBP:Alb1-Arx1 complex was purified using amylose resin and Ni–NTA chromatography, followed by ion exchange and size exclusion chromatography. Purification of the Alb1-Arx1 complex was performed similarly, but the purification on amylose resin was omitted and the MBP-tag was cleaved using TEV protease after the ion exchange chromatography step. The complete purification protocol can be found in the **Supplemental Experimental Procedures**.

Complex formation, cryo-EM specimen preparation, and electron microscopy

Complexes were assembled in 20 mM HEPES-KOH pH 8, 100 mM NaCl, 5 mM $MgCl_2$, 5 mM β-mercaptoethanol using 75 nM purified 60S subunits and the 1-1.5 μM of associated factors (Arx1, Alb1, and Rei1). The sample was applied to glow-discharged holey carbon grids, and plunge-frozen in a liquid ethane-propane mixture (Tivol et al., 2008) at the temperature of liquid N_2 after manual blotting. Cryo-EM data were acquired as described (Greber et al., 2014a) using the EPU software on a Titan Krios cryo-transmission electron microscope (operated at 300 keV) equipped with a Falcon II camera (all FEI Company). Images were acquired at 100'720 x magnification using dose fractionation (movie mode) with a total dose of 20 electrons/$Å^2$. Movie frame alignment was performed using UCSF DRIFTCORR (Li et al., 2013). The complete description of sample preparation and cryo-EM imaging can be found in the **Supplemental Experimental Procedures**.

Data processing

Initial data processing, including movie frame realignment (Li et al., 2013), estimation of CTF parameters (CTFFIND3) (Mindell and Grigorieff, 2003), and particle picking (EMAN 1.9) (Ludtke et al., 1999) was performed as described (Greber et al., 2014a). Further image processing, including 2D classification, 3D classification, and high-resolution refinement was performed in RELION 1.3 (Scheres, 2012) and optimized to classify for the presence of Arx1 at the polypeptide tunnel exit (**Figures S1, S3, S5**). Particles selected during classification were subjected to high-resolution "gold standard" refinement, ensuring independence of the reconstructions from data-half sets (Rosenthal and Henderson, 2003; Scheres, 2012; Scheres and Chen, 2012), to obtain the final reconstructions. Final refinement of the 60S-Arx1-Alb1-Rei1H_6 complex resulted in a reconstruction at 3.4 Å resolution. For dataset sizes and numbers of selected particles, see **Figures S1, S3, S5**. The complete description of cryo-EM data processing and map calculations can be found in the **Supplemental Experimental Procedures**.

Atomic model building and refinement

Atomic model building was performed in O (Jones et al., 1991) (proteins) and COOT (Emsley et al., 2010) (60S subunit rRNA). Refinement and validation of the atomic coordinates was performed using PHENIX as described (Greber et al., 2014a). The complete description of model building and refinement procedures can be found in the **Supplemental Experimental Procedures**.

Chemical crosslinking and mass spectrometry

Chemical crosslinking with disuccinimidyl suberate (DSS) and mass spectrometric analysis were performed on isolated Arx1-Alb1 complexes as well as the 60S-Arx1-Alb1-Rei1 complex as described (Greber et al., 2014a; Greber et al., 2014b). Further details can be found in the **Supplemental Experimental Procedures**.

Yeast genetics, analysis of mutant strains, polysome analysis, and fluorescence microscopy

Saccharomyces cerevisiae strains and plasmids are listed in **Tables S4** and **S5**. Yeast transformations, creation of mutant strains and recombinant DNA techniques were performed according to established procedures. For fluorescence microscopy experiments, cells were incubated for 3 hours at 20°C, harvested by centrifugation, and visualized using a DM6000B microscope (Leica, Germany). Polysome analysis of yeast lysates was performed by sucrose gradient ultracentrifugation as described previously (Altvater et al., 2014). Further details can be found in the **Supplemental Experimental Procedures**.

ACCESSION NUMBERS

The cryo-EM maps of the 60S-Arx1-Alb1-Rei1H_6, 60S-Arx1-Alb1-H_6Rei, and 60S-Arx1-Rei1H_6 complexes have been deposited in the Electron Microscopy Databank (EMDB) with accession codes EMD-3151, EMD-3152, and EMD-3153, respectively. The refined atomic coordinates of the 60S-Arx1-Alb1-Rei1H_6 and 60S-Arx1-Alb1-H_6Rei1 complexes have been deposited at the Protein Data Bank (PDB) with PDB codes 5APO and 5APN.

SUPPLEMENTAL INFORMATION

Supplemental information includes Supplemental Experimental Procedures, six figures and five tables and can be found with this article online at XXXX.

AUTHOR CONTRIBUTIONS

B.J.G. performed complex assembly and specimen preparation for cryo-EM. B.J.G. and D.B. acquired cryo-EM data. B.J.G. processed cryo-EM data with the support of D.B. B.J.G. and M.L. built the atomic models. B.J.G., D.B., M.L., and N.B. interpreted the atomic models. S.G. performed yeast genetics, biochemistry and fluorescence microscopy experiments in the laboratory of V.G.P. M.S. cloned, expressed and purified the Alb1-Arx1 and MBP:Alb1-Arx1 complexes in the laboratory of N.L. A.L. performed CX-MS experiments in the laboratory of R.A. B.J.G. drafted the manuscript and all authors contributed to its final version.

ACKNOWLEDGMENTS

Cryo-EM data were acquired at the Scientific Center for Optical and Electron Microscopy (ScopeM) at ETH Zurich. We thank P. Tittmann (ScopeM) for support. We thank T. Schaefer and S. Arpagaus for support in protein cloning and expression, Martin Altvater for generous help with fluorescence microscopy experiments, and A. Geerlof (EMBL) for providing the petM41 vector. We acknowledge the use of the Euler cluster at the Swiss National Supercomputing Centre of ETH Zurich. This work was supported by the Swiss National Science Foundation (SNSF) and the National Center for Excellence in Research (NCCR) RNA and Disease program of the SNSF, the European Research Council grant 250071 under the European Community's Seventh Framework Programme (to N.B.), the ERC Starting Grant EURIBIO 260676 (to V.G.P.), and the European Research Council (ERC-2008-AdG 233226) (R.A.). B.G. was supported by an Advanced Postdoc.Mobility fellowship from the SNSF (project 160983). Work at Université Paris Descartes was supported by CNRS, University Paris Descartes, the RNPGenesis grant from the Agence Nationale de la Recherche (ANR JC RNPGenesis), the Institut Universitaire de France.

COMPETING FINANCIAL INTERESTS

The authors declare no competing financial interests.

REFERENCES

Altvater, M., Chang, Y., Melnik, A., Occhipinti, L., Schütz, S., Rothenbusch, U., Picotti, P., and Panse, V.G. (2012). Targeted proteomics reveals compositional dynamics of 60S pre-ribosomes after nuclear export. Mol Syst Biol *8*, 628.

Altvater, M., Schütz, S., Chang, Y., and Panse, V.G. (2014). Dissecting ribosome assembly and transport in budding yeast. Methods Cell Biol *122*, 437-461.

Bassler, J., Klein, I., Schmidt, C., Kallas, M., Thomson, E., Wagner, M.A., Bradatsch, B., Rechberger, G., Strohmaier, H., Hurt, E.*, et al.* (2012). The conserved Bud20 zinc finger protein is a new component of the ribosomal 60S subunit export machinery. Mol Cell Biol *32*, 4898-4912.

Ben-Shem, A., Garreau de Loubresse, N., Melnikov, S., Jenner, L., Yusupova, G., and Yusupov, M. (2011). The structure of the eukaryotic ribosome at 3.0 Å resolution. Science *334*, 1524-1529.

Bradatsch, B., Katahira, J., Kowalinski, E., Bange, G., Yao, W., Sekimoto, T., Baumgärtel, V., Boese, G., Bassler, J., Wild, K.*, et al.* (2007). Arx1 functions as an unorthodox nuclear export receptor for the 60S preribosomal subunit. Mol Cell *27*, 767-779.

Bradatsch, B., Leidig, C., Granneman, S., Gnädig, M., Tollervey, D., Böttcher, B., Beckmann, R., and Hurt, E. (2012). Structure of the pre-60S ribosomal subunit with nuclear export factor Arx1 bound at the exit tunnel. Nat Struct Mol Biol *19*, 1234-1241.

Bussiere, C., Hashem, Y., Arora, S., Frank, J., and Johnson, A.W. (2012). Integrity of the P-site is probed during maturation of the 60S ribosomal subunit. J Cell Biol *197*, 747-759.

Demoinet, E., Jacquier, A., Lutfalla, G., and Fromont-Racine, M. (2007). The Hsp40 chaperone Jjj1 is required for the nucleo-cytoplasmic recycling of preribosomal factors in Saccharomyces cerevisiae. RNA *13*, 1570-1581.

Emsley, P., Lohkamp, B., Scott, W.G., and Cowtan, K. (2010). Features and development of Coot. Acta Crystallogr D Biol Crystallogr *66*, 486-501.

Finch, A.J., Hilcenko, C., Basse, N., Drynan, L.F., Goyenechea, B., Menne, T.F., González Fernández, A., Simpson, P., D'Santos, C.S., Arends, M.J.*, et al.* (2011). Uncoupling of GTP hydrolysis from eIF6 release on the ribosome causes Shwachman-Diamond syndrome. Genes Dev *25*, 917-929.

Gerhardy, S., Menet, A.M., Peña, C., Petkowski, J.J., and Panse, V.G. (2014). Assembly and nuclear export of pre-ribosomal particles in budding yeast. Chromosoma *123*, 327-344.

Giglione, C., Boularot, A., and Meinnel, T. (2004). Protein N-terminal methionine excision. Cell Mol Life Sci *61*, 1455-1474.

Greber, B.J., Boehringer, D., Leibundgut, M., Bieri, P., Leitner, A., Schmitz, N., Aebersold, R., and Ban, N. (2014a). The complete structure of the large subunit of the mammalian mitochondrial ribosome. Nature *515*, 283-286.

Greber, B.J., Boehringer, D., Leitner, A., Bieri, P., Voigts-Hoffmann, F., Erzberger, J.P., Leibundgut, M., Aebersold, R., and Ban, N. (2014b). Architecture of the large subunit of the mammalian mitochondrial ribosome. Nature *505*, 515-519.

Greber, B.J., Boehringer, D., Montellese, C., and Ban, N. (2012). Cryo-EM structures of Arx1 and maturation factors Rei1 and Jjj1 bound to the 60S ribosomal subunit. Nat Struct Mol Biol *19*, 1228-1233.

Ho, J.H., Kallstrom, G., and Johnson, A.W. (2000). Nmd3p is a Crm1p-dependent adapter protein for nuclear export of the large ribosomal subunit. J Cell Biol *151*, 1057-1066.

Hung, N.-J., and Johnson, A.W. (2006). Nuclear recycling of the pre-60S ribosomal subunit-associated factor Arx1 depends on Rei1 in Saccharomyces cerevisiae. Mol Cell Biol *26*, 3718-3727.

Hung, N.-J., Lo, K.-Y., Patel, S.S., Helmke, K., and Johnson, A.W. (2008). Arx1 is a nuclear export receptor for the 60S ribosomal subunit in yeast. Mol Biol Cell *19*, 735-744.

Iwase, M., and Toh-e, A. (2004). Ybr267w is a new cytoplasmic protein belonging to the mitotic signaling network of Saccharomyces cerevisiae. Cell Struct Funct *29*, 1-15.

Jones, T.A., Zou, J.Y., Cowan, S.W., and Kjeldgaard, M. (1991). Improved methods for building protein models in electron density maps and the location of errors in these models. Acta Crystallogr A Found Crystallogr *47 (Pt 2)*, 110-119.

Karbstein, K. (2013). Quality control mechanisms during ribosome maturation. Trends Cell Biol *23*, 242-250.

Kaschner, L.A., Sharma, R., Shrestha, O.K., Meyer, A.E., and Craig, E.A. (2015). A conserved domain important for association of eukaryotic J-protein co-chaperones Jjj1 and Zuo1 with the ribosome. Biochim Biophys Acta *1853*, 1035-1045.

Kemmler, S., Occhipinti, L., Veisu, M., and Panse, V.G. (2009). Yvh1 is required for a late maturation step in the 60S biogenesis pathway. J Cell Biol *186*, 863-880.

Klinge, S., Voigts-Hoffmann, F., Leibundgut, M., Arpagaus, S., and Ban, N. (2011). Crystal structure of the eukaryotic 60S ribosomal subunit in complex with initiation factor 6. Science *334*, 941-948.

Klinge, S., Voigts-Hoffmann, F., Leibundgut, M., and Ban, N. (2012). Atomic structures of the eukaryotic ribosome. Trends Biochem Sci *37*, 189-198.

Kowalinski, E., Bange, G., Bradatsch, B., Hurt, E., Wild, K., and Sinning, I. (2007). The crystal structure of Ebp1 reveals a methionine aminopeptidase fold as binding platform for multiple interactions. FEBS Lett *581*, 4450-4454.

Kramer, G., Boehringer, D., Ban, N., and Bukau, B. (2009). The ribosome as a platform for co-translational processing, folding and targeting of newly synthesized proteins. Nat Struct Mol Biol *16*, 589-597.

Lebreton, A., Saveanu, C., Decourty, L., Rain, J.-C., Jacquier, A., and Fromont-Racine, M. (2006). A functional network involved in the recycling of nucleocytoplasmic pre-60S factors. J Cell Biol *173*, 349-360.

Leidig, C., Bange, G., Kopp, J., Amlacher, S., Aravind, A., Wickles, S., Witte, G., Hurt, E., Beckmann, R., and Sinning, I. (2013). Structural characterization of a eukaryotic chaperone--the ribosome-associated complex. Nat Struct Mol Biol *20*, 23-28.

Leidig, C., Thoms, M., Holdermann, I., Bradatsch, B., Berninghausen, O., Bange, G., Sinning, I., Hurt, E., and Beckmann, R. (2014). 60S ribosome biogenesis requires rotation of the 5S ribonucleoprotein particle. Nat Commun *5*, 3491.

Li, X., Mooney, P., Zheng, S., Booth, C.R., Braunfeld, M.B., Gubbens, S., Agard, D.A., and Cheng, Y. (2013). Electron counting and beam-induced motion correction enable near-atomic-resolution single-particle cryo-EM. Nat Meth *10*, 584-590.

Lo, K.-Y., Li, Z., Bussiere, C., Bresson, S., Marcotte, E.M., and Johnson, A.W. (2010). Defining the pathway of cytoplasmic maturation of the 60S ribosomal subunit. Mol Cell *39*, 196-208.

Lo, K.-Y., Li, Z., Wang, F., Marcotte, E.M., and Johnson, A.W. (2009). Ribosome stalk assembly requires the dual-specificity phosphatase Yvh1 for the exchange of Mrt4 with P0. J Cell Biol *186*, 849-862.

Ludtke, S.J., Baldwin, P.R., and Chiu, W. (1999). EMAN: semiautomated software for high-resolution single-particle reconstructions. J Struct Biol *128*, 82-97.

Menne, T.F., Goyenechea, B., Sánchez-Puig, N., Wong, C.C., Tonkin, L.M., Ancliff, P.J., Brost, R.L., Costanzo, M., Boone, C., and Warren, A.J. (2007). The Shwachman-Bodian-Diamond syndrome protein mediates translational activation of ribosomes in yeast. Nat Genet *39*, 486-495.

Merl, J., Jakob, S., Ridinger, K., Hierlmeier, T., Deutzmann, R., Milkereit, P., and Tschochner, H. (2010). Analysis of ribosome biogenesis factor-modules in yeast cells depleted from pre-ribosomes. In Nucleic Acids Research, pp. 3068-3080.

Meyer, A.E., Hoover, L.A., and Craig, E.A. (2010). The cytosolic J-protein, Jjj1, and Rei1 function in the removal of the pre-60 S subunit factor Arx1. J Biol Chem *285*, 961-968.

Meyer, A.E., Hung, N.-J., Yang, P., Johnson, A.W., and Craig, E.A. (2007). The specialized cytosolic J-protein, Jjj1, functions in 60S ribosomal subunit biogenesis. Proc Natl Acad Sci USA *104*, 1558-1563.

Mindell, J.A., and Grigorieff, N. (2003). Accurate determination of local defocus and specimen tilt in electron microscopy. J Struct Biol *142*, 334-347.

Panse, V.G., and Johnson, A.W. (2010). Maturation of eukaryotic ribosomes: acquisition of functionality. Trends Biochem Sci *35*, 260-266.

Parnell, K.M., and Bass, B.L. (2009). Functional redundancy of yeast proteins Reh1 and Rei1 in cytoplasmic 60S subunit maturation. Mol Cell Biol *29*, 4014-4023.

Pertschy, B., Saveanu, C., Zisser, G., Lebreton, A., Tengg, M., Jacquier, A., Liebminger, E., Nobis, B., Kappel, L., van der Klei, I.*, et al.* (2007). Cytoplasmic recycling of 60S preribosomal factors depends on the AAA protein Drg1. In Mol Cell Biol, pp. 6581-6592.

Rabl, J., Leibundgut, M., Ataide, S.F., Haag, A., and Ban, N. (2011). Crystal structure of the eukaryotic 40S ribosomal subunit in complex with initiation factor 1. Science *331*, 730-736.

Raue, U., Oellerer, S., and Rospert, S. (2007). Association of Protein Biogenesis Factors at the Yeast Ribosomal Tunnel Exit Is Affected by the Translational Status and Nascent Polypeptide Sequence. Journal of Biological Chemistry *282*, 7809-7816.

Rigaut, G., Shevchenko, A., Rutz, B., Wilm, M., Mann, M., and Séraphin, B. (1999). A generic protein purification method for protein complex characterization and proteome exploration. Nat Biotechnol *17*, 1030-1032.

Rosenthal, P.B., and Henderson, R. (2003). Optimal determination of particle orientation, absolute hand, and contrast loss in single-particle electron cryomicroscopy. J Mol Biol *333*, 721-745.

Scheres, S.H.W. (2012). RELION: implementation of a Bayesian approach to cryo-EM structure determination. J Struct Biol *180*, 519-530.

Scheres, S.H.W., and Chen, S. (2012). Prevention of overfitting in cryo-EM structure determination. Nat Meth *9*, 853-854.

Stelter, P., Huber, F.M., Kunze, R., Flemming, D., Hoelz, A., and Hurt, E. (2015). Coordinated Ribosomal L4 Protein Assembly into the Pre-Ribosome Is Regulated by Its Eukaryote-Specific Extension. Mol Cell *58*, 854-862.

Tivol, W.F., Briegel, A., and Jensen, G.J. (2008). An improved cryogen for plunge freezing. Microsc Microanal *14*, 375-379.

van Noort, V., Bradatsch, B., Arumugam, M., Amlacher, S., Bange, G., Creevey, C., Falk, S., Mende, D.R., Sinning, I., Hurt, E.*, et al.* (2013). Consistent mutational paths predict eukaryotic thermostability. BMC Evol Biol *13*, 7.

Walzthoeni, T., Leitner, A., Stengel, F., and Aebersold, R. (2013). Mass spectrometry supported determination of protein complex structure. Curr Opin Struct Biol *23*, 252-260.

Yao, W., Roser, D., Köhler, A., Bradatsch, B., Bassler, J., and Hurt, E. (2007). Nuclear export of ribosomal 60S subunits by the general mRNA export receptor Mex67-Mtr2. Mol Cell *26*, 51-62.

Yao, Y., Demoinet, E., Saveanu, C., Lenormand, P., Jacquier, A., and Fromont-Racine, M. (2010). Ecm1 is a new pre-ribosomal factor involved in pre-60S particle export. RNA *16*, 1007-1017.

Zhang, Y., Ma, C., Yuan, Y., Zhu, J., Li, N., Chen, C., Wu, S., Yu, L., Lei, J., and Gao, N. (2014). Structural basis for interaction of a cotranslational chaperone with the eukaryotic ribosome. Nat Struct Mol Biol *21*, 1042-1046.

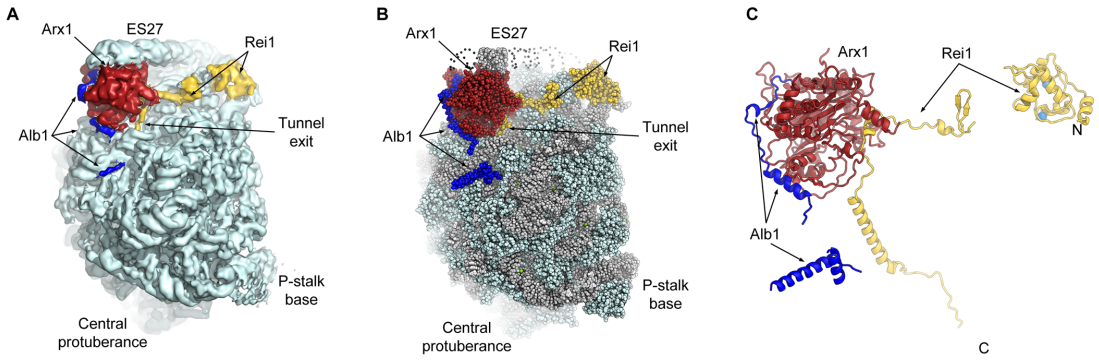

Figure 1. The structure of the 60S-Arx1-Alb1-Rei1H$_6$ complex.

A, Cryo-EM reconstruction of Rei1 (yellow) and the Arx1-Alb1 complex (red and blue, respectively) bound to the 60S subunit (cyan). Cryo-EM map low-pass filtered to 6.5 Å resolution for clarity. **B**, Refined coordinate model of the 60S-Arx1-Alb1-Rei1H$_6$ complex colored as in **A**, but with the rRNA shown in grey. ES27 is indicated schematically. **C**, The structure of the associated factors. Two zinc atoms in the zinc finger domains of Rei1 are shown as light blue spheres.

See also Figures S1, S2 and Tables S1, S2.

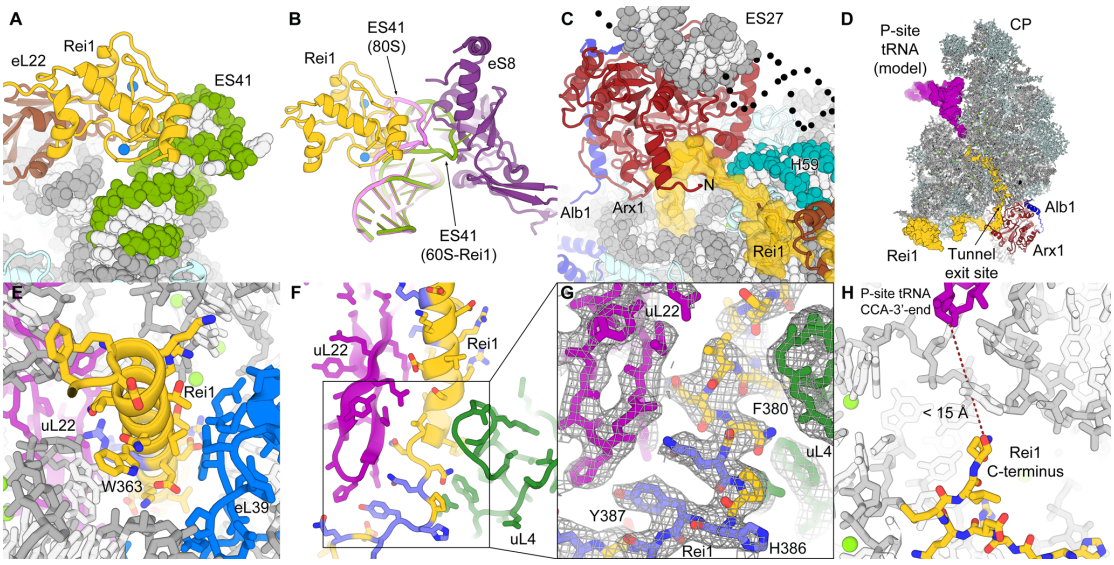

Figure 2. The structure of Rei1.

A, The second and third zinc finger domains of Rei1 (yellow, zinc atoms blue) interact with eL22 (brown) and ES41 (green). **B**, Comparison of the ES41 conformations in the 60S-Rei1 complex (green) and the 80S ribosome (ES41 pink; PDB ID 4V88 (Ben-Shem et al., 2011)). **C**, Interaction of the penultimate α-helix of Rei1 near the N-terminal helix of Arx1 (red) close to rRNA H59 (teal). **D**, Superposition of a P-site tRNA (purple surface) onto the structure of the 60S-Arx1-Alb1-Rei1H_6 complex shown in section to reveal the Rei1 C-terminal domain (yellow surface) inside the exit tunnel. **E**, Rei1 residues 353-377 (yellow) form a plug-like α-helix that interacts with the rRNA as well as uL22 (purple) and eL39 (blue) near the exit of the ribosomal tunnel. **F**, **G**, Details of the Rei1 C-terminal sensor domain and its interactions with the tunnel wall near the constriction site of the ribosomal tunnel (uL4 in green, uL22 in purple; highly conserved residues of Rei1 in slate blue; rRNA and other proteins omitted for clarity). The cryo-EM density is shown as mesh in **G**. **H**, The C-terminus of Rei1 (yellow sticks) reaches to within 15 Å of the 3'-end of the modeled tRNA positioned in the PTC (see **D**). The structure of the 60S-Arx1-Alb1-H_6Rei1 complex has been used for this panel (see **Figure S3**).

See also Figures S3, S4.

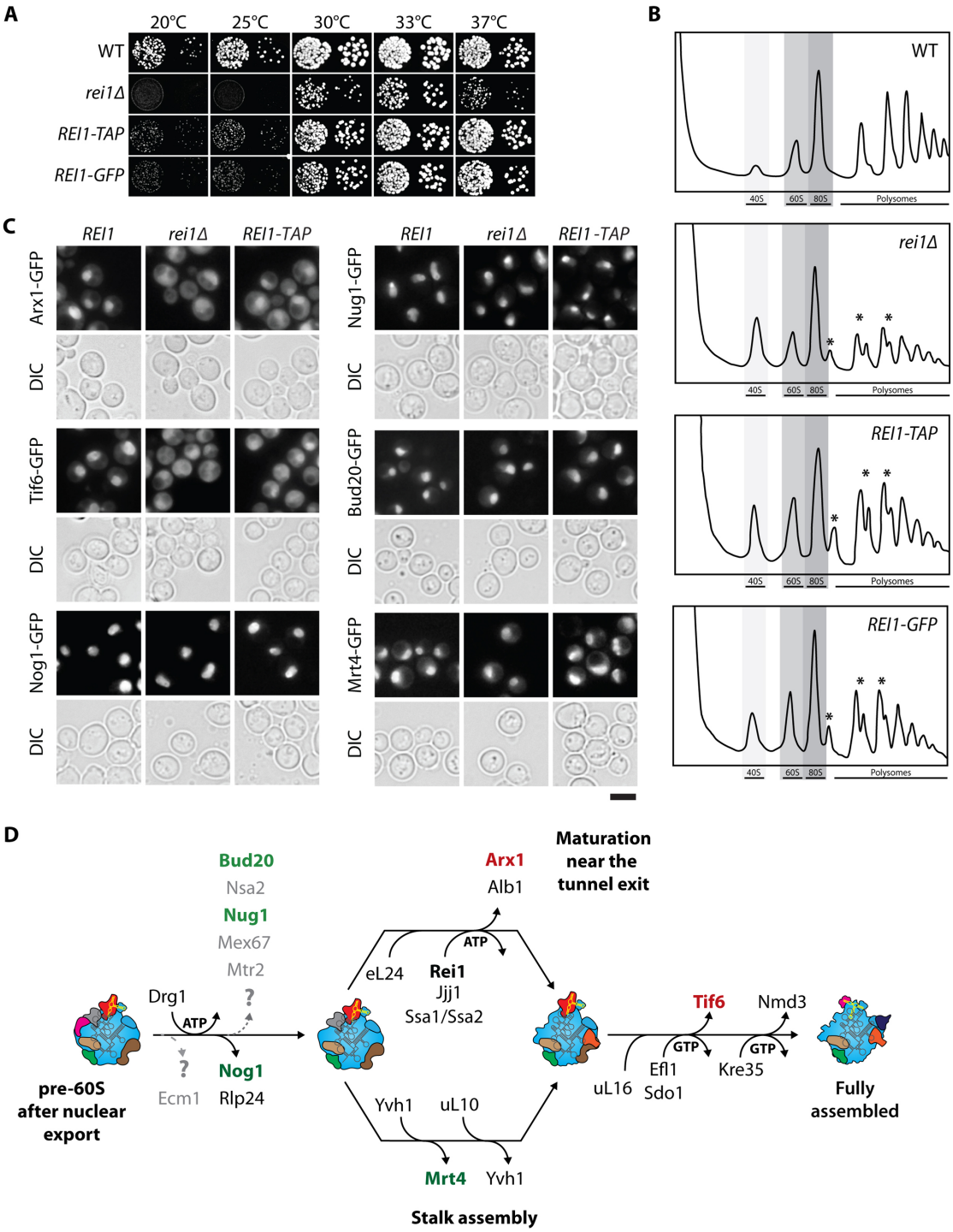

Figure 3. Functional analysis of the Rei1 C-terminal sensor domain.

A, Fusion of a TAP-tag or a GFP moiety to the C-terminus of Rei1 causes a cold-sensitive slow growth phenotype in mutant yeast cells. **B**, Sucrose gradient profiles show an increase of free 40S subunits and the appearance of half-mer peaks in *REI1-TAP* and *REI1-GFP* cells, similar to *rei1Δ* cells. **C**, Fluorescence microscopy shows mislocalization of Arx1-GFP and Tif6-GFP from the nucleus to the cytoplasm in *REI1-TAP* cells while the localization of Bud20, Nug1, Nog1, and

Mrt4 remains unaffected. Scale bar: 5 µm. **D**, Simplified schematic of cytoplasmic 60S maturation. In Rei1 mutants, recycling of Arx1 and Tif6 (red) is impaired, while factors involved in earlier maturation steps or stalk assembly (green) are properly recycled.

See also Tables S4, S5.

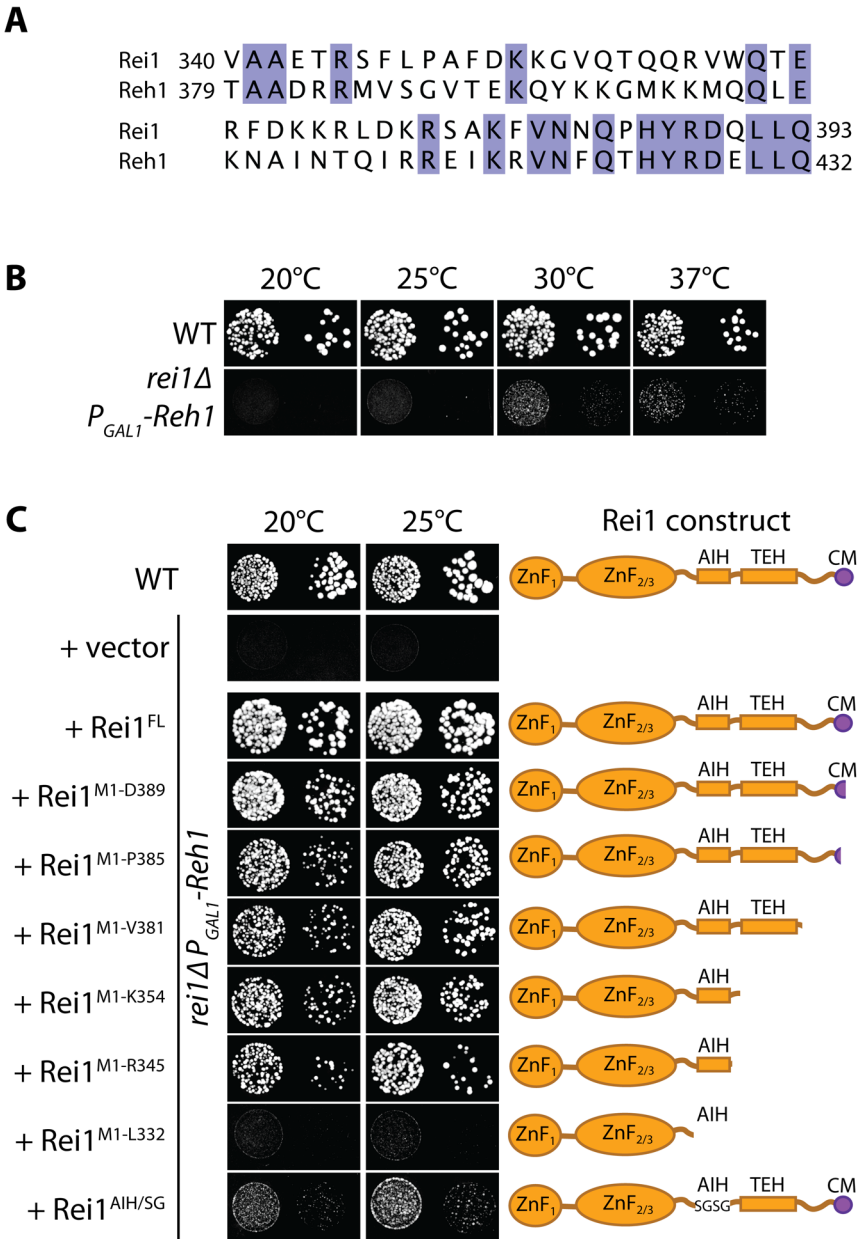

Figure 4. Analysis of Rei1 C-terminal deletion variants. A, Sequence alignment of the C-terminal regions of yeast Rei1 and Reh1 reveals a high degree of conservation in the C-terminal 15 aa. **B**, The *rei1Δ* P_{GAL1}-Reh1 double depletion strain exhibits a strong growth defect on glucose medium at all temperatures tested. **C**, The growth defect of the *rei1Δ* P_{GAL1}-Reh1 strain is only partially complemented by truncated Rei1 variants at low temperatures. Rei1 variants used are schematically indicated on the right. ZnF: zinc finger; AIH: Arx1 interacting helix; TEH: tunnel exit helix (last helix of Rei1, inserted near the tunnel exit); CM: conserved motif (C-terminal 10 aa conserved in Rei1 from yeast to humans, see **Figure S4G**); SGSG: AIH replaced by Ser-Gly linker.

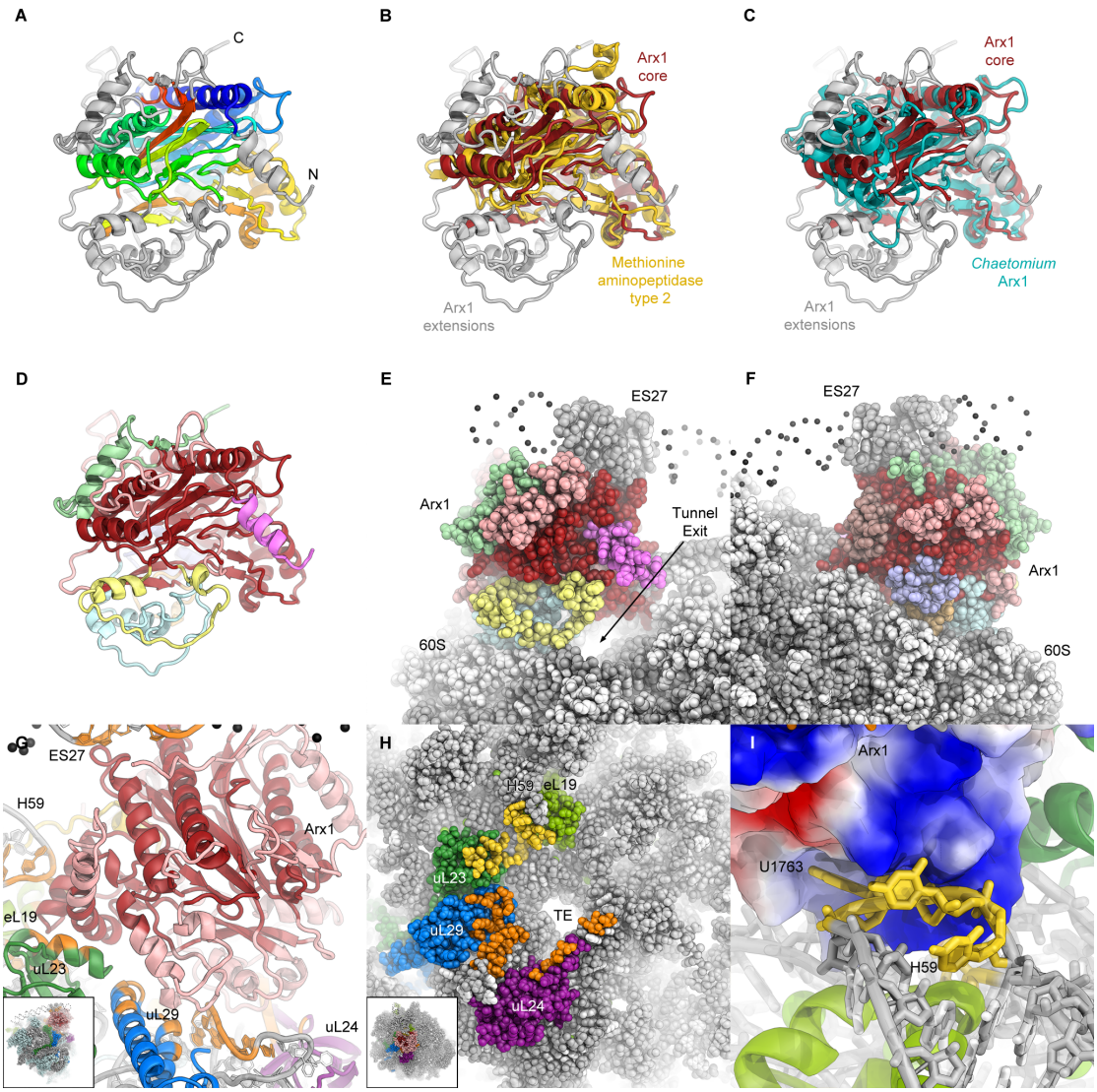

Figure 5. Structure of Arx1 and interactions with the 60S subunit.

A, The conserved type 2 MAP core fold of Arx1 is depicted using a spectrum of colors from N-terminus (blue) to C-terminus (red). Extensions of the core fold are colored in grey. **B**, **C**, Superposition of the structure of Arx1 (red, extensions grey) with type 2 MAP (yellow, PDB ID 1KQ9) (**B**) and *Chaetomium thermophilum* Arx1 (cyan, PDB ID 4IPA) (**C**). **D**-**F**, Arx1 (core in red) with major extensions colored in yellow, cyan, slate blue, brown, and pink and remaining smaller loop extensions in light red. 60S subunit shown in grey in (**E**, **F**). **G**, Arx1 (core fold red, extensions light red) interacts with uL23, uL24, uL29, and eL19 (green, purple, blue, and light green, respectively) as well as the rRNA in the vicinity of the tunnel exit. 60S residues involved in contacts are shown in orange. **H**, Contact sites of Arx1 on the 60S subunit. Ribosomal proteins are colored as in **G**. Residues forming interactions with the Arx1 core fold are colored yellow,

those interacting with Arx1 extensions orange. **I**, Interaction of Arx1 (shown as electrostatic potential surface) with H59. In addition to formation of electrostatic interactions, U1763 of the 25S rRNA is bound in a pocket of Arx1.
See also Figure S4.

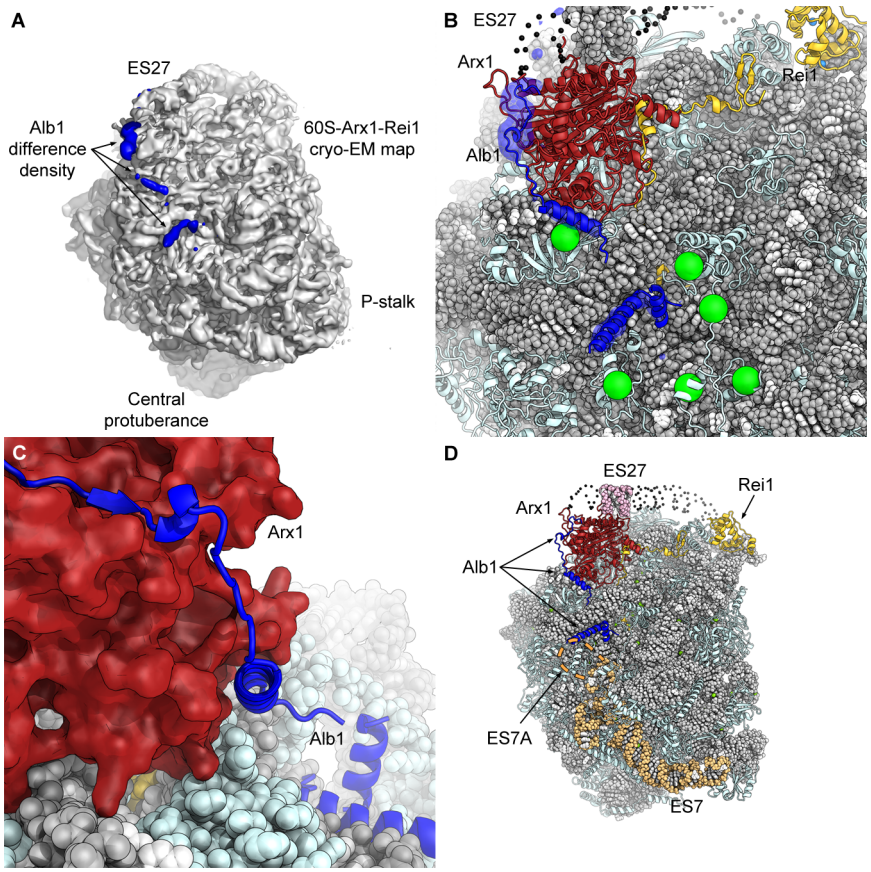

Figure 6. Localization and interactions of Alb1.

A, Difference density corresponding to Alb1 (blue) was obtained by subtracting the density of the 60S-Arx1-Rei1H_6 complex (grey) from the 60S-Arx1-Alb1-Rei1H_6 complex. **B**, Positioning of secondary structure elements of Alb1 (blue) in the 60S-Arx1-Alb1-Rei1H_6 complex. Green spheres indicate Alb1 crosslinking sites on ribosomal proteins from CX-MS experiments (**Table S3**). Alb1 difference density shown as semi-transparent surface. **C**, Interaction of an Alb1 α-helix (blue) with a groove formed by Arx1 (red). **D**, The Arx1-Alb1 complex (red and blue) sits in between ES27 (pink) and ES7 (orange)

See also Figures S5, S6 and Table S3.

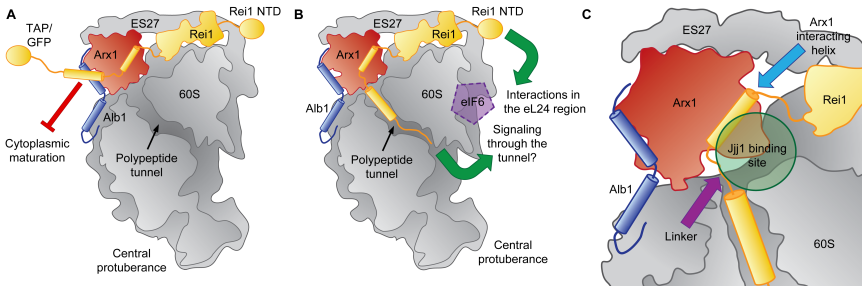

Figure 7. Release of Arx1 and Rei1 from the pre-60S particle and cytoplasmic 60S maturation.

A, Fusion of a bulky moiety to the Rei1 C-terminus prevents insertion into the tunnel and blocks 60S cytoplasmic maturation. **B**, Due to the insertion of its C-terminus into the ribosomal tunnel, Rei1 is able to approach the 60S subunit interface from two sides (green arrows; Rei1 NTD: Rei1 N-terminal domain not visualized in our maps). The approximate location of 60S-bound eIF6 (Tif6) is indicated (purple pentagon). **C**, Release of Arx1 and Rei1 from the pre-60S particle. The Rei1 helix interacting with Arx1 (cyan arrow) or the linker connecting this helix to the Rei1 domain in the tunnel (purple arrow) are located in the immediate vicinity of the Jjj1 binding site (Greber et al., 2012) (green disc) and are possible points of action for Jjj1-Ssa during release of Arx1 and Rei1 from the pre-60S particle.